PNAS RESEARCH ARTICLE | CELL BIOLOGY OPEN ACCESS

Tubuloid culture enables long-term expansion of functional human kidney tubule epithelium from iPSC-derived organoids

Fjodor A. Yousef Yengej[a,b], Jitske Jansen[c,d,e], Carola M. E. Ammerlaan[a,b], Emre Dilmen[f], Carla Pou Casellas[a,b], Rosalinde Masereeuw[g], Joost G. Hoenderop[f], Bart Smeets[c], Maarten B. Rookmaaker[b], Marianne C. Verhaar[b,1,2], and Hans Clevers[a,1,2,3]

Contributed by Hans Clevers; received October 2, 2022; accepted December 29, 2022; reviewed by Seppo Vainio and James M. Wells

Kidney organoids generated from induced pluripotent stem cells (iPSC) have proven valuable for studies of kidney development, disease, and therapeutic screening. However, specific applications have been hampered by limited expansion capacity, immaturity, off-target cells, and inability to access the apical side. Here, we apply recently developed tubuloid protocols to purify and propagate kidney epithelium from d7+18 (post nephrogenesis) iPSC-derived organoids. The resulting 'iPSC organoid-derived (iPSCod)' tubuloids can be exponentially expanded for at least 2.5 mo, while retaining expression of important tubular transporters and segment-specific markers. This approach allows for selective propagation of the mature tubular epithelium, as immature cells, stroma, and undesirable off-target cells rapidly disappeared. iPSCod tubuloids provide easy apical access, which enabled functional evaluation and demonstration of essential secretion and electrolyte reabsorption processes. In conclusion, iPSCod tubuloids provide a different, complementary human kidney model that unlocks opportunities for functional characterization, disease modeling, and regenerative nephrology.

kidney | organoid | tubuloid | stem cells | electrolyte transport

Significance

The kidneys have highly complex architectures and functions. Advanced models are therefore required to push research into human kidney development, function, disease, and regeneration forward. Organoids from induced pluripotent stem cells and tubuloids grown from adult stem/progenitor cells are two novel models that have proven valuable for these purposes. These models each have their specific advantages and uses. Here, both protocols are combined to generate 'iPSCod tubuloids', a different laboratory model of the kidney with complementary advantages to both organoids and tubuloids. iPSCod tubuloids are easily handled and display key kidney functions such as waste excretion and salt reabsorption. We expect that this approach will prove useful for future research into human kidney function and disease.

The renal tubular epithelium plays a crucial role in kidney function by fine-tuning the composition of the glomerular filtrate via selective secretion and reabsorption of circulating compounds. Dysfunction of the tubular epithelium results in a wide variety of diseases. Moreover, the renal tubular epithelium is the target of many frequently prescribed drugs. Due to the high complexity of the nephron, advanced in vitro models are required to study its development and function in health and disease. In the past decade, pluripotent stem cell (PSC)-derived kidney organoids and adult stem/progenitor cell (ASPC)-based tubuloids grown from the primary renal epithelium have emerged as powerful in vitro models of the human nephron (1–4). These complementary models each offer specific advantages and applications (5).

Organoids are grown from either embryonic stem cells or induced PSC (iPSC) by mimicking embryonic development of the kidney. First, PSCs are differentiated to mesoderm-derived ureteric bud (UB) and metanephric mesenchyme (MM) using exogenous signals. The renal precursor tissues then exchange reciprocal endogenous signals to autonomously form podocytes, tubular epithelium, vasculature, and stromal cells organized in nephron-like structures (1, 2, 6–8). Human kidney organoids have been used for a variety of purposes, including studies of organ development, disease modeling, drug efficacy and toxicity testing, and first steps toward regenerative medicine (8–18). These applications have been facilitated by introduction of knockouts and reporters (9, 11, 14, 19–21). However, specific applications are hindered by loss of expansion capacity, as well as accumulation of fibrosis and cyst formation upon long-term culture (beyond around day d7+18, depending on the protocol) (20, 22–24). Furthermore, although protocols have already achieved directed differentiation of PSCs up to first and second trimester fetal kidney tissues, further maturation is warranted to study the adult kidney. Besides that protocols not only generate mainly renal cell types but also off-target cells from the mesoderm (e.g., cardiac muscle, reproductive system) and other germ layers (e.g., neuronal and melanoma-like cells), as well as undifferentiated cells that together can add up to around 20% of cells (6–8, 17, 25). Finally, the nephron-like architecture is an exceptional accomplishment and provides many merits, yet complicates apical access of the tubular epithelium required for e.g., studies of epithelial transport.

Tubuloid culture applies signals involved in physiological turnover and regeneration in the adult kidney to permit durable expansion of the primary renal epithelium derived from renal biopsies or urine (4, 5, 26). The resulting cultures consist of the mature tubular epithelium, without vasculature or stroma, nor off-target cells, which is beneficial for e.g., functional analysis and modeling disorders in tubular transport (4, 5). Tubuloids were recently developed and have so far been used to gain insights into kidney turnover, assess nephrotoxicity, and produce

[1]To whom correspondence may be addressed. Email: m.c.verhaar@umcutrecht.nl or h.clevers@hubrecht.eu.

[2]M.C.V. and H.C. contributed equally to this work.

[3]Present address: Pharma, Research and Early Development (pRED) of F. Hoffmann-La Roche Ltd, 4070 Basel, Switzerland.

This article contains supporting information online at https://www.pnas.org/lookup/suppl/doi:10.1073/pnas.2216836120/-/DCSupplemental.

Published February 1, 2023.

disease models with subsequent therapeutic screening (4, 27–32). Easy efficient establishment and expansion from patient urine makes tubuloids amenable for personalized medicine and biobanking as well (4, 28, 33, 34). Drawbacks include the lack of reported genome editing (e.g., by CRISPR-Cas9) protocols in tubuloids and the absence of podocytes, vasculature, and stroma that play important roles in specific aspects of kidney (patho)physiology.

Here, we combine the advantages of both models by applying tubuloid culture protocols to differentiated iPSC kidney organoids [Takasato protocol d7+18 (1)] to generate 'iPSC organoid-derived (iPSCod) tubuloids'. A similar approach has proven effective for intestinal organoids (35). The resulting cultures selectively expand the mature functional renal epithelium without off-target cells and provide easy apical access that enables evaluation of tubular transport. iPSCod tubuloids provide a different in vitro model of the human kidney with complementary features.

Results

Kidney Organoids Lose Renal Tubules and Become Fibrotic during Long-Term Culture. Kidney organoids, grown using the protocol by Takasato et al., reach their optimal form around d7+18, with physiologically organized glomerular-like (Nephrin+) and tubular (Lotus Tetragonolobus Lectin(LTL)+, E-cadherin(CAD)+) structures (*SI Appendix*, Fig. S1 *A–C*) (1). Continued culture beyond that point results in deterioration. In d7+40 organoids, the no. of LTL+ and ECAD+ tubules decreased and ki67+ proliferating cells disappeared (*SI Appendix*, Fig. S1 *A–D*). Prolonged cultures developed interstitial fibrosis (*SI Appendix*, Fig. S1 *E* and *F*), and structural organization diminished (*SI Appendix*, Fig. S1*G*). These findings are in line with previous reports (20, 22–24).

iPSCod Tubuloid Culture Enables Isolation and Long-Term Propagation of Organoid-Derived Kidney Epithelium. To isolate and expand the renal epithelium beyond d7+18, tubuloid protocols were applied on kidney organoids. First, iPSCs were differentiated to organoids using the protocol by Takasato et al. (1). Briefly, iPSCs were differentiated to UB and mM in twodimensional (2D) culture, and then at d7 these embryonic kidney precursor cells were reaggregated on Transwell™ plates, where they exchange signals that simulate further differentiation and self-organization into nephron structures that resemble the first-second trimester fetal kidney at d7+18 (1, 6). The d7+18 organoids were then dissociated by enzymatic digestion. The fragments were embedded in basement membrane gel and supplied with growth factors involved in tubuloid culture and renal turnover in vivo as previously described (4, 36–38). This resulted in emergence of three-dimensional cultures named 'iPSCod tubuloids' within 1 wk (Fig. 1*A*). In this way, three iPSCod tubuloid cultures (lines 4, 5, and 7) were established on different time points from three different batches of renal organoids grown from iPSC. These lines were successfully expanded, frozen, and thawed, and were used for the experimental work in this study. In early passages, these cultures mostly consisted of folded structures (resembling parts of tubules in d7+18 organoids), which gradually changed to spherical structures, similar to tubuloids from primary kidney tissue (4). iPSCod tubuloids were cultured for up to 16 passages (4 mo), with weekly 1:3 split ratios that provide exponential expansion (i.e., one well can be expanded to $6.6 \times 10^{\wedge 3}$ wells in 8 wk) (Fig. 1 *A* and *B*). The presence of abundant ki67+ cells further substantiates that iPSCod tubuloids maintain proliferative capacity on the long-term (Fig. 1*C*). Around passage 13 (over 3 mo of culture), the morphology changed and expansion potential diminished (Fig. 1*B*).

Transmission electron microscopy revealed that iPSCod tubuloids consist of the polarized epithelium, with a basolateral basement membrane and an apical brush border. Some structures displayed typical proximal tubular invaginations, and the presence of transported material in the lumen hints at proximal tubular function (Fig. 1*D*).

iPSCod Tubuloids Retain Expression of Key Tubular Transporters and Transcription Factors over Long-Term Culture. Over long-term culture, iPSCod tubuloids preserve different tubular cell types with expression of genes and proteins required for function. Expanding and differentiated iPSCod tubuloids in passage 1 (d7+18+14), 3 (d7+18+28), 6 (d7+18+49), and 9 (d7+18+70) were compared with iPSC-derived organoids at d7+18, d7+32, and d7+40. iPSCod tubuloids retained tubular cell types from the proximal tubule (PT), thick ascending limb of the loop of Henle (TAL), distal convoluted tubule (DT), and principal cells (PC) of the collecting duct, as indicated by expression (upon differentiation) of specific markers such as, respectively, hepatocyte nuclear factor 4α (HNF4α), Na/K/2Cl-cotransporter 2 (NKCC2), Na/Cl cotransporter (NCC), aquaporin 2 (AQP2), bulk mRNA, and protein (Fig. 2 *A* and *B* and *SI Appendix*, Fig. S2). The reduction in Nephrin expression over weeks of culture indicates loss of podocytes over time in the iPSCod cultures (Fig. 2*A*). The clustering of segment-specific stainings within one structure suggests that each iPSCod tubuloid typically represented a specific nephron segment (Fig. 2*B*).

Within these cell types, expression of key genes and proteins involved in function (and disease) was preserved over months of exponential expansion. These included the PT-specific transcription factors HNF1α and HNF4α and the bicarbonate reclamation transporter NBCe1 (*SLC4A4*) (39). In the distal segments, transporters required for reabsorption of electrolytes and water were conserved, including NKCC2 (*SLC12A1,* TAL), the epithelial Na channel α (ENaCα, *SCNN1A,* PC) and AQP2 (PC) (Fig. 2 *A* and *B*). NKCC2 and AQP2 expression started to decrease around, respectively, passages 9 and 6. These transcriptomic data were reinforced by immunohistochemistry confirming consistent NKCC2 protein expression between passages 2 and 6, but loss of AQP2 in passage 6 (*SI Appendix*, Fig. S2*B*). Of note, expression of *HNF1A*, *HNF4A*, NBCe1, NKCC2, and ENaCα diminished in organoids during culture beyond d7+18 (Fig. 2*A*).

iPSCod Tubuloid Culture Removes Immature and Off-Target Cell Types. Organoids contain populations of cells that are only present during embryonic kidney development, including *OSR1*+ intermediate mesoderm, *GDNF*+ mM, *SIX2*+ cap mesenchyme, *LGR5*+ loop of Henle progenitors, and *FOXD1*+ stromal progenitors (40, 41). Indeed, these genes were highly expressed in iPSC-derived organoids, whereas they were barely expressed in iPSCod tubuloids over passages 1 to 9 (Fig. 3*A*). Proteins required for function in mature tubular cells were stably expressed in iPSCod tubuloids (Fig. 2 *A* and *B*). Together, these data indicate that iPSCod tubuloid culture enriches for the mature renal epithelium.

Common off-target cell types in iPSC kidney organoids include neuronal cells, cardiomyocytes, and muscle cells. Top differentially expressed markers that characterize these cells include *STMN2, ZIC2,* and *TUBB3* for neuronal cells, *TNNT2* (cardiac troponin T) for cardiomyocytes, and *TNNC2* (troponin C) and *MYH3* (myosin 3) for muscle (6, 8, 17, 25). We observed loss of expression of these genes in iPSCod tubuloid passage 1 and onward, indicating rapid removal of off-target cells (Fig. 3*B*).

iPSCod tubuloids do not accumulate fibrosis over long-term expansion. Whereas collagen I production contributed to the basement membrane of d7+18 tubuloids, excessive deposits in d7+40 organoids resulted in fibrosis (Figs. 1 *B*, *E*, and *F* and 4*C*). In iPSCod tubuloid cultures (up to at least passage 6), collagen I

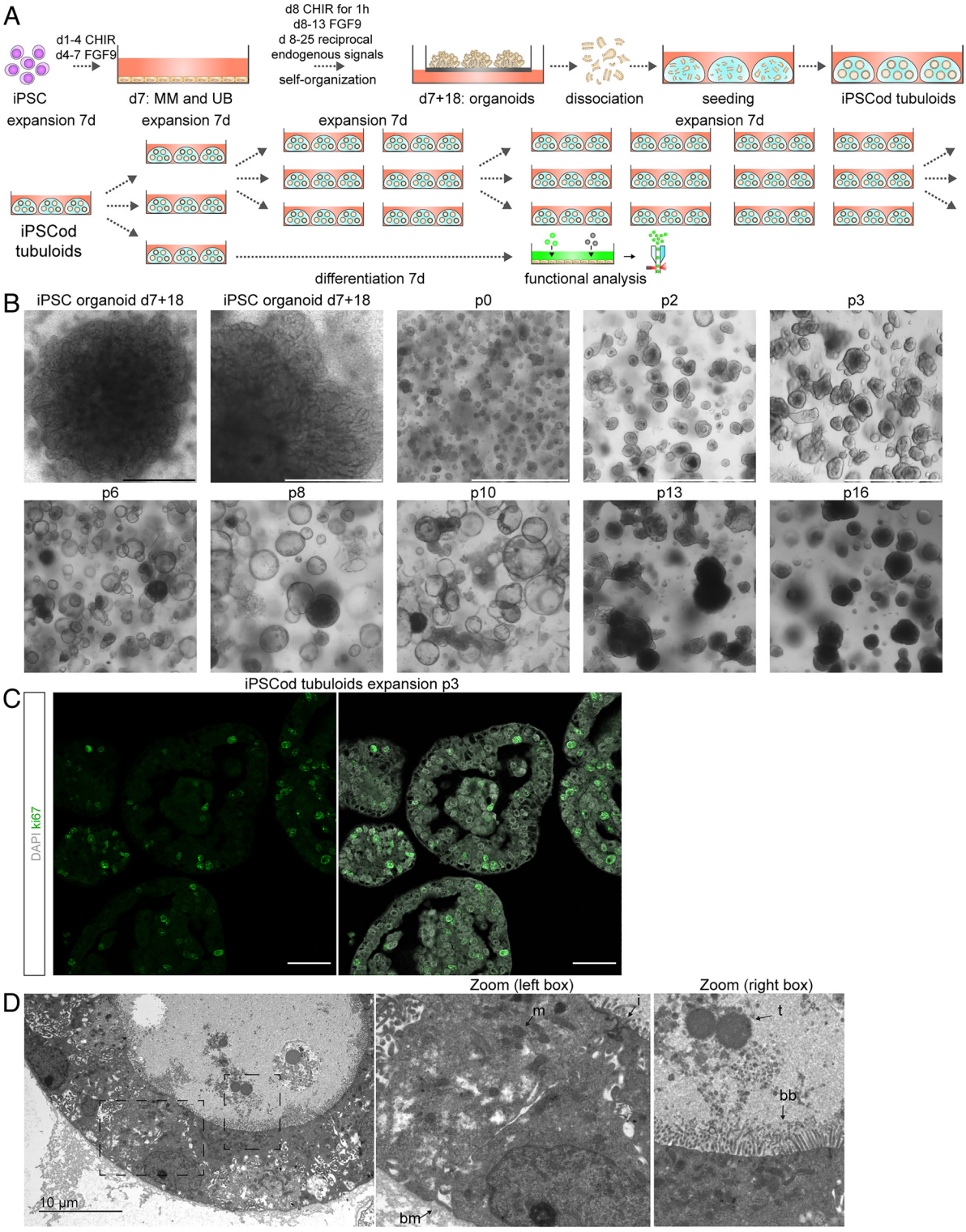

Fig. 1. iPSCod tubuloid culture enables long-term expansion of kidney organoid-derived human renal epithelium. (*A*) Graphic summary of the differentiation of iPSCs to kidney organoids and subsequent establishment of iPSCod tubuloid cultures, subsequent expansion, and use in experiments. d = day, h = hour. (*B*) Brightfield images of iPSC organoids at d7+18 and thereof derived iPSCod tubuloid cultures over 16 passages (every passage represents about 1 wk culture). Black scale bar = 2,000 µm. White scale bar = 1,000 µm. (*C*) Expression of the proliferation marker ki67 in iPSCod tubuloids in passage 3 and 6. (Scale bar, 50 µm.) (*D*) Transmission electron microscopy images of differentiated iPSCod tubuloids. *Left*: PT epithelium. *Right*: distal epithelium. bb = brush border. i = invaginations. m = mitochondria. t = material indicative of transport (apical excretion). bm = basement membrane.

remained confined to the basement membrane and did not cause formation of fibrotic tissue (Fig. 3*C*).

iPSCod Tubuloid Epithelium Is Leak-Tight and Capable of Secretion and Electrolyte Reabsorption. iPSCod tubuloids can produce leak-tight 2D monolayers that provide apical access required for functional evaluation of luminal transport and related diseases. Leak-tightness is an important prerequisite for selective transport and therefore epithelial function. Leak-tightness of iPSCod tubuloids grown as 2D monolayers on Transwell™ filters was demonstrated by high

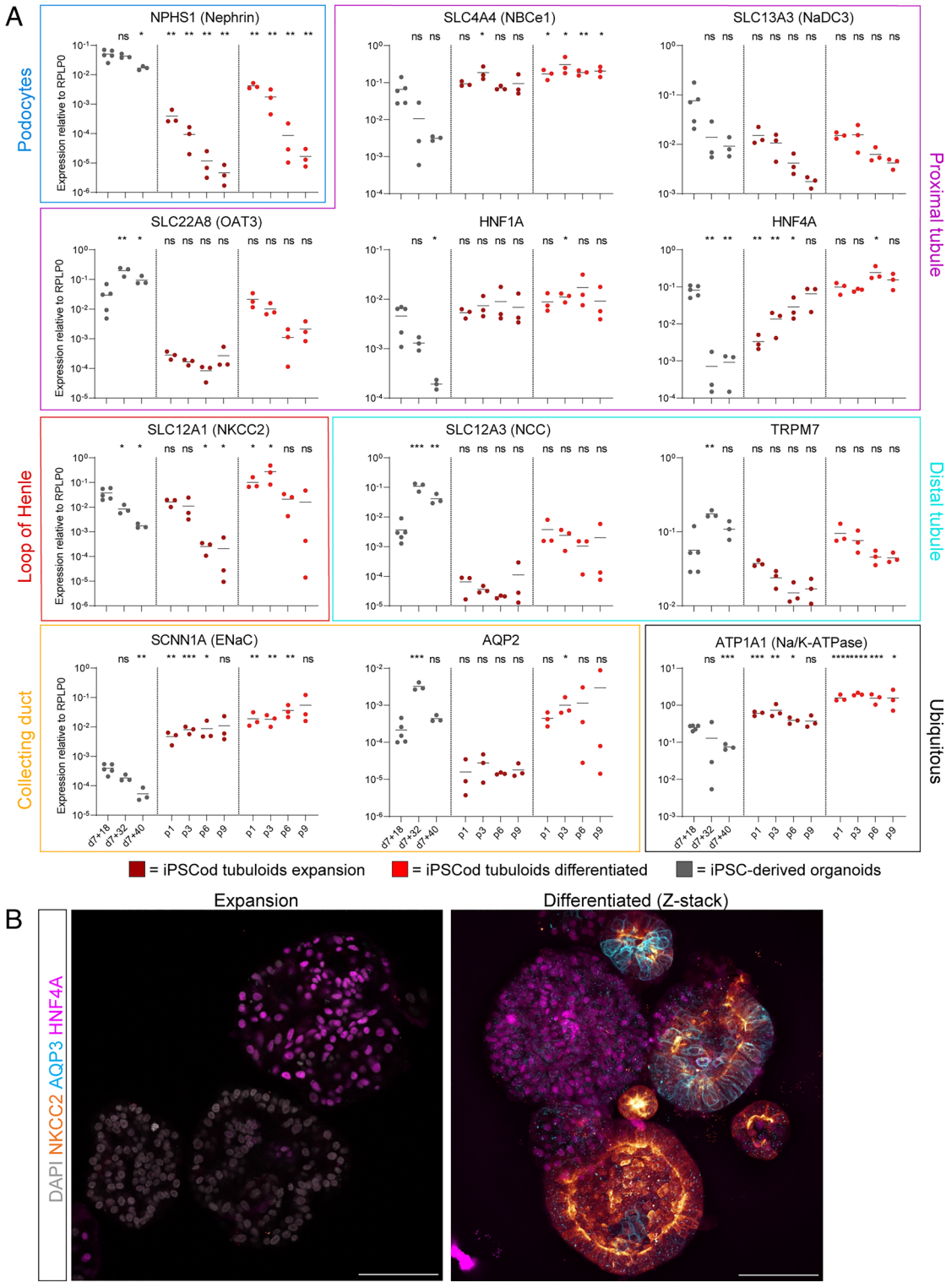

Fig. 2. iPSCod tubuloids retain expression of key transcription factors and transporters over long-term culture. (*A*) Normalized mRNA expression of a variety of cell type markers, transcription factors, and transport proteins across the nephron. iPSCod tubuloids in expansion and differentiation conditions over 9 passages (n = 3 lines) were compared with iPSC-derived kidney organoids harvested at d7+18, d7+32, and d7+40 (n ≥ 3 batches of organoids). Different iPSCod lines and passages within lines, as well as different batches of organoids were harvested on different time points. (*B*) Immunofluorescence images confirm expression of various relevant transporters in iPSCod tubuloids on protein level. (Scale bar, 100 μm.)

transepithelial electrical resistance (TEER) values combined with absent leakage of 2 to 5-kDa inulin-fluorescein isothiocyanate (FITC) (Fig. 4 *A* and *B*). Inulin is a polysaccharide that is neither (re)absorbed nor secreted by the kidney epithelium and therefore well suited to study tubular paracellular leakage in vitro (in addition to traditional use in measurement of glomerular filtration in vivo) (42, 43).

To assess whether the iPSCod tubuloid epithelium is capable of selective excretion, the 2D monolayer was basolaterally exposed to 5(6)-carboxy-2′,7′-dichlorofluorescein diacetate (CDFDA). After diffusion into the cells, this compound is hydrolyzed to CDF, a substrate of the multidrug resistance protein 2 and 4 (MRP2/4) efflux pumps that remove xenobiotics

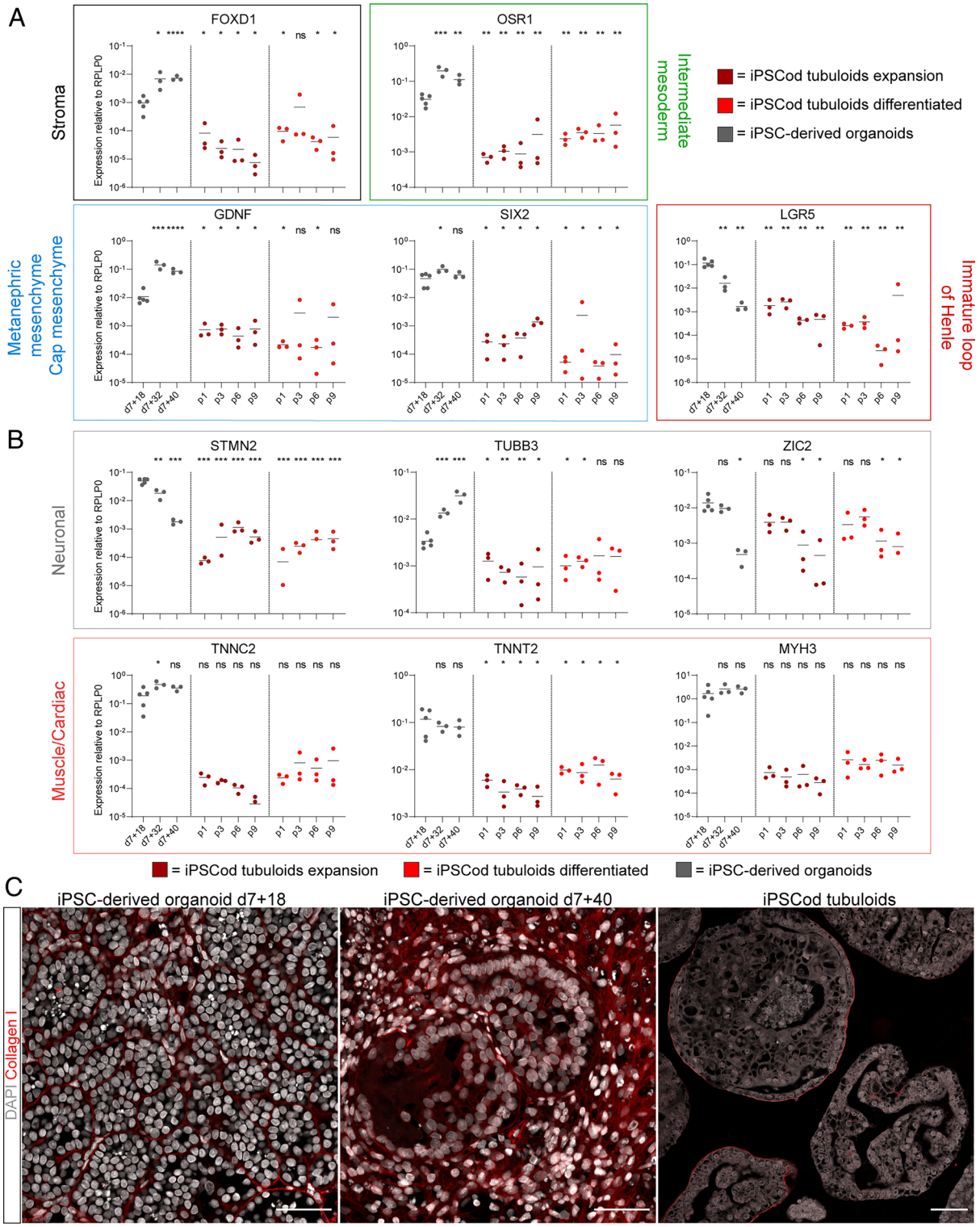

Fig. 3. iPSCod tubuloid culture removes immature and off-target cells, and prevents fibrosis. Normalized mRNA expression of markers that characterize renal embryonic stromal, mesenchymal, and epithelial cells (*A*) and unfavorable off-target cells and profibrotic cells (*B*). iPSCod tubuloids in expansion and differentiation conditions over 9 passages (n = 3 lines) were compared with iPSC-derived kidney organoids harvested at d7+18, d7+32, and d7+40 (n ≥ 3 batches of organoids). Different iPSCod lines and passages within lines, as well as different batches of organoids were harvested on different time points. (*C*) Collagen I staining in iPSCod tubuloids and iPSC-derived organoids at d7+18 and d7+40. (Scale bar, 50 μm.)

(waste products, drugs, toxins) in the kidney in vivo (44). After 45 min, CDF was detected apically, indicating luminal efflux. The MRP2/4 inhibitor MK571 inhibited luminal CDF efflux (Fig. 4*C*) and caused intracellular accumulation (Fig. 4*D*). These data show that iPSCod tubuloids are capable of MRP2/4-mediated excretion.

2D grown monolayers expressed polarized Na^+ transport proteins such as luminal NKCC2 and basolateral Na/K-ATPase (Fig. 5*A*). The iPSCod tubuloid epithelium was capable of reabsorption of apical $^{22}Na^+$. Uptake was enhanced by exposure to hypotonic low Cl^- buffer similar to in vivo, demonstrating that Na^+ transport is responsive to physiological stimuli (45–47). Reabsorption was

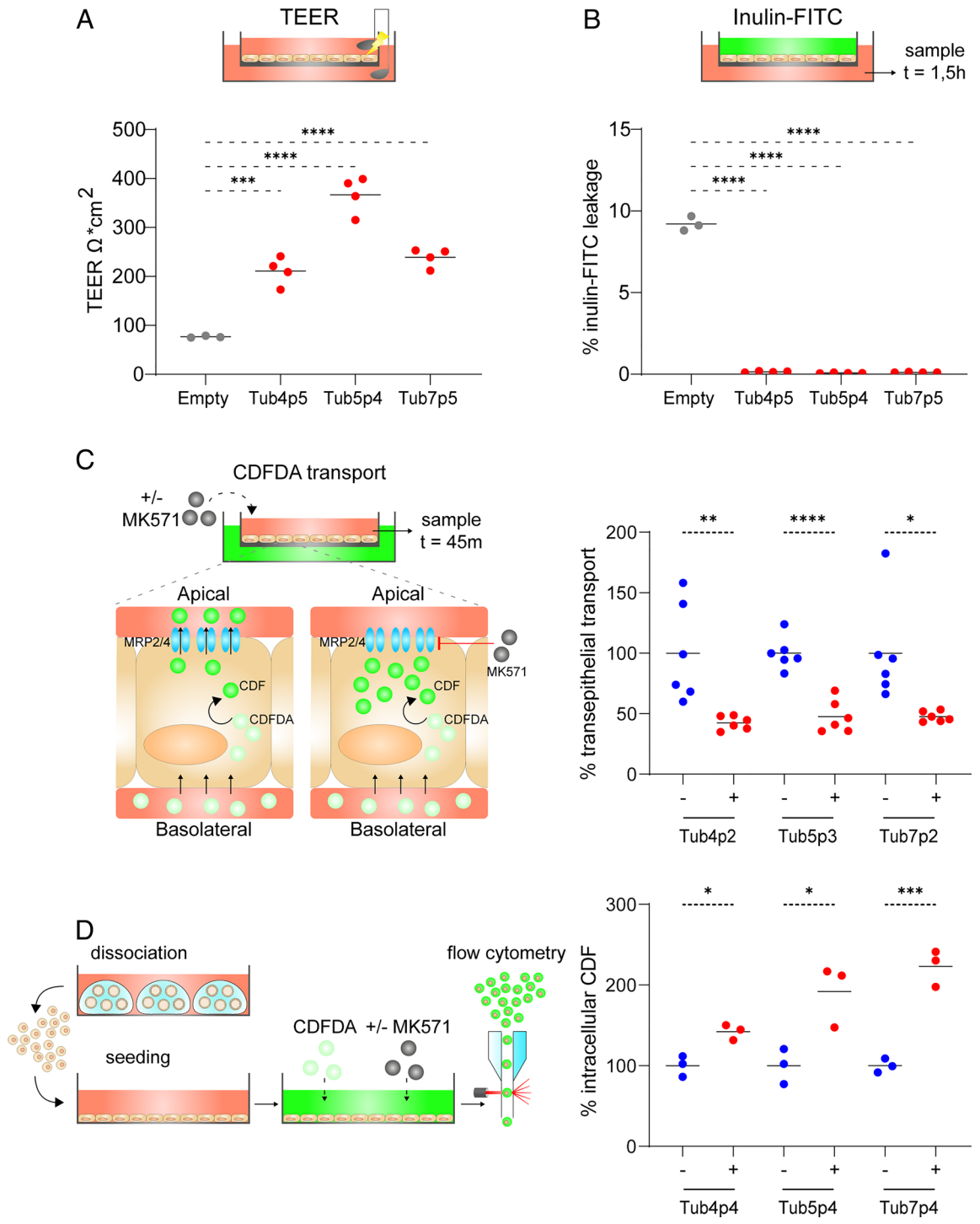

Fig. 4. iPSCod tubuloid epithelium is leak-tight and capable of luminal MRP2/4-mediated secretion. (*A*, *B*) Assessment of leak-tightness of the iPSCod tubuloid epithelium in Transwells™ by measurement of the TEER and inulin-FITC leakage (n = 3 lines, four technical replicates each, analyzed together at the same time). (*C*) *Left*: Graphic summary of analysis of transepithelial transport and MRP2/4-mediated apical efflux using a Transwell™ system. iPSCod tubuloids were cultured in Transwells™ and exposed to CDFDA (which is intracellularly metabolized to the MRP2/4 substrate CDF) in the presence and absence of the MRP2/4 inhibitor MK571. *Right*: % transepithelially transported CDF in iPSCod tubuloids in the presence and absence of MK571 (n = 3 lines, 2 Transwells™/condition for each line with three technical replicates/Transwell™, analyzed together at the same time). (*D*) *Left*: Graphic summary of analysis of MRP2/4-mediated excretory function using flow cytometry. iPSCod tubuloids were cultured in 2D and exposed to CDFDA +/− MK571. Intracellular CDF accumulation was measured using flow cytometry. *Right*: % CDF accumulation in iPSCod tubuloids (n = 3 lines, analyzed together at the same time) in the presence and absence of MK571. Increased signal shows CDF accumulation (which is expected upon inhibition of apical efflux using MK571). **P* < 0.05, ***P* < 0.01, ****P* < 0.001, and *****P* < 0.0001.

inhibited using the diuretics bumetanide, thiazide, and amiloride that inhibit NKCC2, NCC, and ENaC, the major distal nephron Na^+ transporters/channels (Fig. 5 *B* and *C*). The Na/K-ATPase inhibitor ouabain was added to all conditions to prevent basolateral removal of absorbed Na^+. When separated, each diuretic inhibited Na^+ reabsorption, with amiloride being the most effective, indicating that electrolyte reabsorption was mediated by NKCC2+ TAL, NCC+ DT cells and in particular ENaC+ PC (Fig. 5*D*). Na^+ transport function was preserved between different iPSCod lines and between passages 3 and 6 (Fig. 5 *C* and *D*).

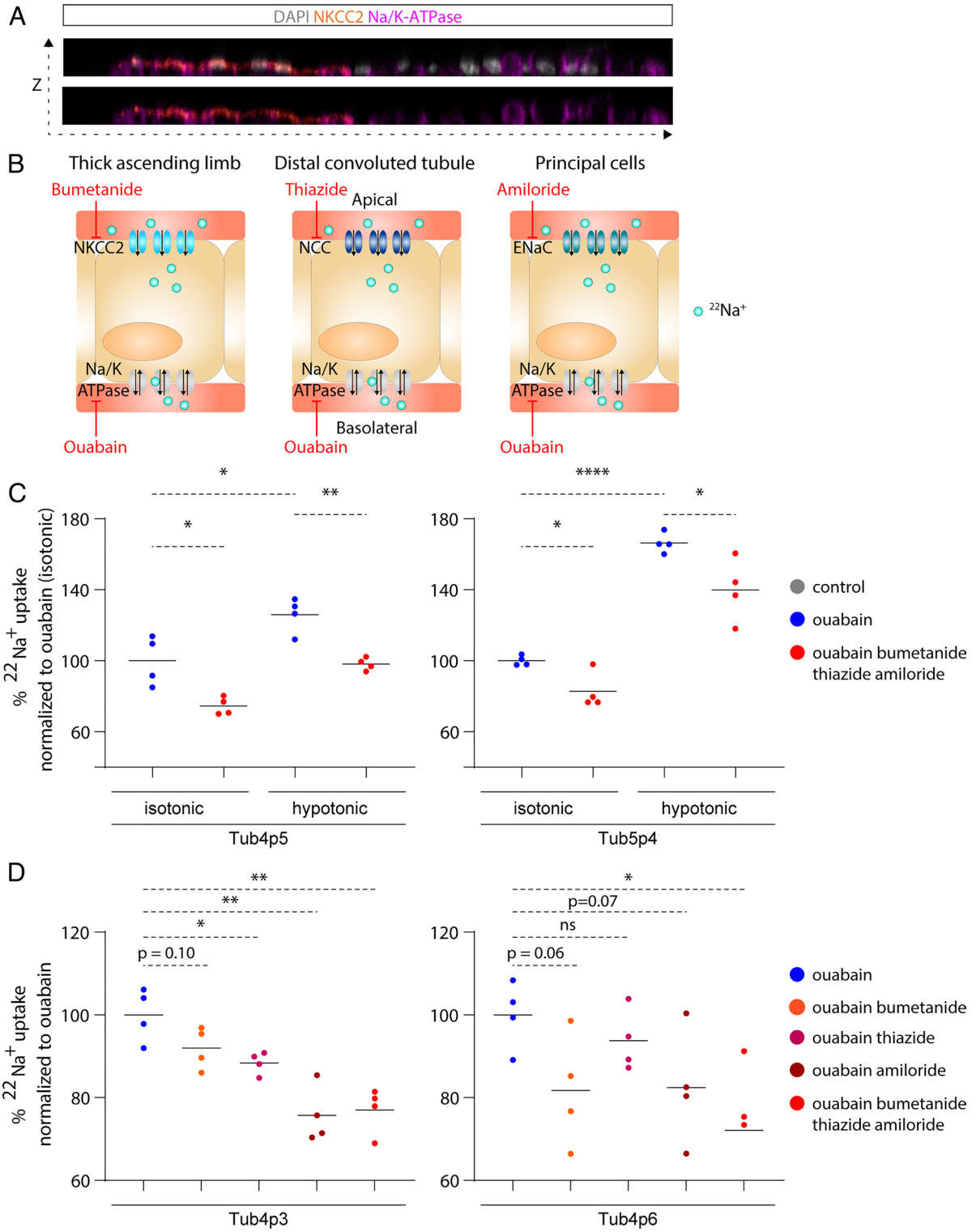

Fig. 5. iPSCod tubuloids demonstrate channel-specific sodium reabsorption. (*A*) Immunofluorescence confirms polarized expression of apical NKCC2 and basolateral Na/K-ATPase in 2D cultured iPSCod tubuloids. (*B*) Graphic summary of electrolyte reabsorption in the TAL, DT, and PC. (*C*, *D*) Reabsorption of $^{22}Na^+$ in isotonic and (uptake stimulating) hypotonic conditions and in the presence and absence of the ouabain, bumetanide, thiazide, and amiloride that, respectively, inhibit the Na/K-ATPase, NKCC2, NCC, and ENaC. Ouabain was used to prevent basolateral removal of absorbed $^{22}Na^+$. *C*: n = 2 lines (each measured on a different day) with four technical replicates per condition. *D*: n = 1 line, two different passages (each measured on a different day) with four technical replicates per condition. $*P < 0.05$, $**P < 0.01$, $***P < 0.001$, and $****P < 0.0001$.

iPSCod Tubuloid Culture Protocols Yield Similar Results when Applied on iPSC Organoids Established from Different iPSC Lines. Finally, to test the reproducibility and broad applicability of this protocol, iPSCod tubuloids grown from different iPSC cell lines were compared. Another iPSCod tubuloid line (no. 9) was successfully established from renal organoids grown from iPSC line 19, and then compared with iPSCod tubuloid lines 4, 5, and 7 (used for the aforementioned experiments) that ultimately originated from iPSC line 15-0001. The resulting iPSCod tubuloids showed similar morphologies (*SI Appendix*, Fig. S3*A*).

Comparable mRNA expression of nephron segment-specific markers and transporters indicates a corresponding distribution of the different nephron segment cell types and reproducible differentiation (*SI Appendix*, Fig. S3*B*). Furthermore, immature cell types and off-target cells were lost in iPSCod line 9, similar to the beneficial effects in lines 4, 5, and 7 (*SI Appendix*, Fig. S3*C*). These data indicate reproducible results when iPSCod tubuloid culture protocols are applied on kidney organoids grown from different iPSC lines.

Discussion

Our results show that, whereas prolonged culture of iPSC-derived organoids results in decreased proliferation, increased fibrosis and persistent presence of off-target cells (1, 6–8, 20, 22–24), switching to the tubuloid culture approach at d7+18 purifies the culture for the mature tubular epithelium, clears it from off-target cells, and rekindles proliferation. Moreover, important transcription factors and transport proteins are preserved over long-term expansion, and the iPSCod tubuloid epithelium enables functional evaluation of both reabsorption and secretion.

There are prominent differences and complementary benefits between iPSC organoids and iPSCod tubuloids. Organoids mimic embryonic morphological development of the whole nephron including the glomerulus, tubule, and interstitial compartment. Whereas the nephron-like architecture of kidney organoids is ideal for testing e.g., morphological development, iPSCod tubuloid culture reduces the model complexity and produces reductionist cultures that can be more easily handled and used to create easy apical (and basolateral) access. Importantly, our iPSCod approach adds a different, easy, and effective strategy to improve maturation and reduce off-target cells to available protocols based on manipulation of signaling pathways and xenotransplantation (6, 12, 22, 25, 48–50). This method also adds a different way to enrich for (various) distal nephron cell types from iPSC organoids to recent protocols that report maturation toward a CD phenotype (12, 48, 49, 51). We took advantage of the apical accessibility to confirm MRP2/4-mediated luminal secretion, a process that follows in vivo after basolateral uptake of uremic toxins and xenobiotics by organic anion and cation transporters in the PT (52). These data complement previous studies that showed the latter process by reporting cisplatin and gentamycin uptake in the PT of iPSC-derived organoids (1, 3, 9). Moreover, we evaluated NKCC2, NCC, and ENaC-mediated electrolyte transport and demonstrate physiologically regulated, diuretic-inhibitable luminal Na^+ reabsorption by human TAL, DT, and PC cells. This represents a central role of the kidney. Interestingly, two very recent studies report amiloride causing changes in transmembrane electrical currents and resistance, indicating ENaC function (51, 53, 54). We add to these data by measuring direct ion transport and testing Na^+ transporters in the LoH (NKCC2) and DT (NCC) in addition to PC ENaC. Together with these studies, our data complement the available functional assays in PSC-derived organoids that focused on glomerular filtration and PT (re)uptake (1, 3, 9, 10, 21, 53). Similar to tubuloids, podocytes disappear in iPSCod tubuloids over the first passages, which probably reflects the poor proliferative potential of these cells in vivo (55, 56). Therefore, organoids from iPSCs are the current model of choice for studies of glomerular disease (10, 18, 50, 57).

Although iPSCod tubuloids share many characteristics with traditional tubuloids, there are some complementary strengths. Next to similar expression of most of the tubule segment markers as reported in regular tubuloids (4), iPSCod tubuloids (especially upon differentiation) show abundant expression of several proximal tubular genes (e.g., HNF1a and HNF4a), the main TAL transporter (NKCC2) and the PC water channel AQP2. Furthermore, human PSCs are an unlimited and easily accessible source of starting material of the same genetic background. Moreover, in future experiments iPSC organoids can be genetically modified by CRISPR-Cas9 to introduce fluorescent reporters or knockouts that provide opportunities for profound interrogation of the role of specific proteins and cell types, as well as artificial introduction of disease models (9, 11, 14, 19–21). Taken together, iPSCod tubuloids combine the advantages of organoids and tubuloids to provide a complementary advanced model of the human kidney tubule.

This approach has several limitations. Expression of some transporters of interest, such as NKCC2 and AQP2 starts to decrease around passages 9 and 6, respectively. Given exponential expansion capacity up to that point and since iPSCs provide an endless source of material, this is easily circumvented for studies looking into the function of these proteins. Second, iPSCod tubuloids provide a heterogeneous population of the tubular epithelium, comparable to tubuloids from the primary tissue (4). However, as demonstrated in this work, the use of specific substrates and inhibitors enables detailed investigation of distinct tubular functions. Furthermore, in future studies techniques such as single-cell RNA-sequencing and multiplex flow cytometry or immunofluorescence (combining read-outs with cell type markers) can be used to study specific cell types. Third, iPSCod tubuloids lose podocytes, vasculature, and interstitial cells (similar to tissue-derived tubuloids). For applications that require these compartments, combination with other approaches (e.g., isolation of these cell populations from cell lines, primary tissue or regular iPSC organoids) is probably required. Finally, we confined our analysis to iPSCod tubuloids established from organoids that were grown using one protocol in the field (1), whereas many different protocols are available that give rise to renal organoids with different cell compositions (2, 12, 18, 48–50, 58, 59). In the future, the differences between iPSCod tubuloids established from different protocols should be compared, in particular for protocols that further mature or enrich for specific cell types (12, 48, 49).

iPSCod tubuloid cultures open interesting avenues for future research. This approach benefits application of iPSC kidney organoids in regenerative nephrology, as it enables exponential expansion, purification (removal of off-target tissue and immature cells), and functional evaluation of the organoid-derived renal epithelium. The persistent proliferative capacity enables studies of renal regeneration in vitro. Compared with tubuloids, it offers the advantage of genetic modification, which could ultimately enable for e.g., transplantation with autologous genetically corrected renal tissue for patients with severe hereditary tubulopathies. Similar to tissue-derived tubuloids, the iPSCod tubuloid epithelium can be seeded not only on Transwells™, but also in more sophisticated organ-on-a-chip systems (33) to evaluate renal epithelial function in a physiological, tubular shape, with and without flow and with apical and basolateral access. These more advanced in vitro models will enable investigation of the interaction between different tissues (e.g., vasculature, interstitial cells) (60, 61). Furthermore, application of the iPSCod tubuloid protocol on organoids from iPSCs with CRISPR-Cas9-induced knockouts or reporters will facilitate functional evaluation of the genetically modified tubular epithelium to study e.g., the function and membrane trafficking of specific (transport) proteins [e.g., NKCC2 (62)] and induced diseases. Finally, this strategy, where ASPC organoid protocols are applied on iPSC-derived organoids to produce iPSCod cultures, has potential for extrapolation to other organs. For example, organoid cultures from human adult and

fetal liver yield remarkably different results (63, 64). iPSCod liver organoids have potential to circumvent the ethical issues of fetal material, while providing comparable benefits.

In conclusion, we present a simple and effective method for isolation, long-term expansion and functional assessment of the mature tubular epithelium from kidney organoids. The resulting iPSCod tubuloids present an advanced in vitro model that combines the advantages of iPSC-derived organoids and tubuloids grown from primary renal tissue to produce a different, complementary model of the human kidney. iPSCod tubuloids demonstrated key tubular functions and hold promise for future evaluation of kidney physiology and disease, drug screening and regenerative nephrology.

Materials & Methods

Human Material. Permission for the creation and use of iPSCs in this study was obtained from the local ethics commission for human-related research of the Radboud university medical center, Nijmegen (approval nos.: 2015-1543 and 2006-048).

iPSC Maintenance Culture. iPSCs (lines 15-0001 and 19) were cultured [as previously described (18)] on Geltrex-coated (ThermoFisher) cell culture plates (Greiner) using Essential™ 8 (E8) medium (Gibco, ThermoFisher) supplemented with E8 supplement (50X, Gibco) and 0.5% (v/v) antibiotic-antimycotic (Gibco). Medium was refreshed daily. Upon 80% confluency, iPSCs were washed using PBS and subsequently split into colonies using PBS-EDTA (0.5 mM, ThermoFisher) for 4 to 6 min at room temperature. Cells were split in a ratio of 1:6—1:8 twice per week.

iPSC-Derived Kidney Organoid Differentiation. iPSCs were seeded in single cells, following TrypLE Select Enzyme (ThermoFisher) for 2 min at 37 °C, on Geltrex-coated cell culture plates using E8 medium supplemented with E8 supplement, 0.5% (v/v) antibiotic-antimycotic, and 1X RevitaCell using a density of 20,000 cells/cm^2. The differentiation protocol was based on Takasato et al. (1). In brief, 24 h post seeding, culture medium was replaced by E6 medium supplemented with 6 μM CHIR (Tocris, Bio-Techne) to initiate differentiation (day 0 to day 4). From day 4 onward, cells were cultured in E6 medium supplemented with FGF9 (200 ng/mL) and heparin (1 ug/mL). At day 7, cells were harvested using trypsin-EDTA (ThermoFisher) and cell aggregates, consisting of 300 K cells per aggregate, were transferred to Transwell™ plates (Corning) and incubated for at least 1 h at 37 °C, 5% (v/v) CO2, with E6 medium supplemented with 5 μM CHIR to induce self-organizing nephrogenesis. After 1 h, the medium was replaced by E6 medium supplemented with FGF9 and heparin and refreshed daily. At day 7+5 (i.e., 5 d post pelleting), E6 medium without any growth factors was used until the end of experiment (i.e., day 7+18, day 7+32, and day 7+40).

iPSCod Tubuloid Culture. Human iPSC-derived organoids at d7+18 were dissociated using Accutase (Thermo Fisher Scientific) at 37 °C for 15 to 20 min. Tubular fragments and cells were washed, resuspended in ice-cold Basement Membrane Extract (BME) gel (R&D systems), and plated on prewarmed suspension culture wells plates. Plates were incubated at 37 °C for at least 30 min to solidify the gel. Tubuloid expansion medium [EM, as previously described (4, 33)] was added. The cultures were incubated at 37 °C with 5% CO_2, and EM was refreshed every 2 to 3 d. After around 7 to 10 d, iPSCod tubuloid structures appeared. These were further maintained in EM and passaged every ~7 d as described before (4, 33). Three iPSCod lines (4, 5, and 7) were established on three different time points from three different batches of kidney organoids grown from iPSC line 15-0001, and later iPSCod line 9 was established from kidney organoids grown from iPSC line 19. These iPSCod tubuloid lines were expanded, passaged (and often also frozen, thawed, and again passaged) before they were used in experiments.

For experiments, iPSCod tubuloids were grown in EM for 2 to 3 d postdissociation (to regrow) and then treated with EM or differentiation medium (as described in ref. 4 supplemented with 10 μM FSK, 5 μM A83-01 and 10 μM fludrocortisone) for 7 d [Yousef Yengej et al. Manuscript under revision].

For 2D and Transwell™ experiments, iPSCod tubuloids were dissociated to single cells and counted as reported for tubuloids (33). Around 100,000 cells in EM were seeded in 12-well or 24-well culture plates, or in 24-well plate 0.4-μm pore polyester Transwell™ membrane inserts (Corning). Cells were grown to confluency in EM, and then the medium was replaced by differentiation medium for 7 d. Cells were cultured and differentiated at 37 °C with 5% CO_2, and media were refreshed every 2 to 3 d.

qPCR. For qPCR experiments, RNA was isolated using the RNEasy kit (Qiagen) according to the manufacturer's instructions. Reverse transcription was done using M-MLV Reverse Transcriptase, RNase H Minus, Point Mutant (Promega) according to the manufacturer's instructions. IQ Sybr Green SuperMix (Bio-Rad) was used for qPCR. For the reaction, a CFX384 Touch Real-Time PCR Detection System (Bio-Rad) was used. Primers were designed using Primer3 (https://primer3.ut.ee/) or the Harvard PrimerBank (https://pga.mgh.harvard.edu/primerbank/). Primer sequences are provided in *SI Appendix*, Table S1.

Immunocytochemistry (ICC) and -histochemistry (IHC). iPSCod tubuloids were collected for ICC (with removal of BME gel), fixed, permeabilized, and stained as described for tubuloids (29). Antibodies used for ICC and IHC are provided in *SI Appendix*, Table S2.

The procedure for immunofluorescence staining of formalin-fixed paraffin-embedded (FFPE) tissue was performed as described by Jansen et al. (18) In brief, deparaffinized slides (4 μm) were boiled in Tris-buffered EDTA antigen retrieval buffer (VWR Chemicals) for 20 min in a microwave. Primary (1:100) and secondary (1:200) antibodies were diluted in PBS containing 1% (v/v) BSA (Sigma-Aldrich). Primary antibodies were incubated overnight at 4 °C, while secondary antibodies were incubated at room temperature for 2 h. Stained slides were mounted using Fluoromount-G® (Southern Biotech, Sanbio). Images were captured using the Zeiss LSM 880 confocal microscope.

Masson's trichrome staining and hematoxylin and eosin (H&E) immunohistochemistry were also performed on iPSC-derived kidney organoid FFPE tissue. To identify matrix production, a trichrome staining was performed using Masson's trichrome staining kit (Sigma-Aldrich) according to the manufacturer's protocol. For H&E staining, deparaffinized slides (4 μm) were stained with 50% hematoxylin solution for 1 to 2 min, rinsed with water, followed by 1% Eosin solution stain for 1 to 2 min, dehydrated, and mounted. Images were captured using a VisionTek Digital Microscope (Sakura FineTek).

Quantification of Fibrosis. Double-blinded interstitial fibrosis scoring was performed of four independent organoid batches (day 7+18 and day 7+40), at least 2 biological replicates per condition (3 areas per replicate were used for scoring). Scoring

grades: 0 = no fibrosis, 1 = mild fibrosis, 2 = moderate fibrosis, 3 = severe fibrosis.

Quantification of Renal Tubules. The quantification of LTL+/ECAD+ signal was performed of four independent organoid batches (day 7+18 and day 7+40), at least 2 biological replicates per condition, using Fiji. Three areas per replicate were used for Fiji quantification. The LTL+ECAD+ signal was corrected for surface area, and data were normalized to day 7+18 organoids.

Evaluation of Leak-Tightness. iPSCod tubuloids were grown in Transwells™, differentiated for 7 d, and then TEER values were measured using the Millicell® ERS-2 Voltohmmeter (Millipore). Resistance values were multiplied by 0.33 cm^2 (Transwell™ surface area) to calculate the TEER in Ω*cm^2.

For measurements of inulin leakage, Transwell™ filters were washed once with Hanks' Balanced Salt solution (HBSS, Gibco) with 1% HEPES (Thermo Fisher Scientific). Then 0.2 mL 0.05 mg/mL 2 to 5 kDa inulin-FITC (Sigma) in HBSS with 1% HEPES was added to the apical side and 0.6 mL HBSS with 1% HEPES. Cells were incubated at 37 °C for 90 min, and then triplicates of 50 µL were sampled from the basolateral compartment and transferred to black flat bottom 96-well chimney plates (Greiner). Fluorescence was measured (λex = 485 nm, λem = 530 nm) using a SPARK multimode microplate reader (TECAN). Baseline fluorescence (HBSS with 1% HEPES) was subtracted from the measured values. % leakage was determined as (triplicate mean basolateral/triplicate mean apical)*100%.

MRP2/4 Transport Function. iPSCod tubuloids were grown in Transwells™ to confluency, differentiated for 7 d, and then leak-tightness was assessed. Transwells™ were washed once with HBSS with 1% HEPES. Then 0.2 mL 10 µM CDFDA (Sigma) +/− 20 µM MK571 (Sigma) in HBSS with 1% HEPES was added apically and HBSS with 1% HEPES +/− 20 µM MK571 basolaterally. Cells were incubated at 37 °C for 45 min, and then triplicates of 50 µL were sampled from the basolateral compartment and transferred to black flat bottom 96-well chimney plates (Greiner). Fluorescence was measured (λex = 485nm, λem = 530 nm) using a SPARK multimode microplate reader (TECAN). Baseline fluorescence (HBSS with 1% HEPES) was subtracted from the measured values. % transport was determined as (apical fluorescence /mean apical fluorescence in the minus MK571 control condition)*100%.

For intracellular CDF measurements, iPSCod tubuloids were seeded in 2D culture plates, grown to confluency, and differentiated for 7 d. Tubuloid epithelium was washed twice with PBS and then apically exposed to HBSS with 1% HEPES + 50 µM CDFDA +/− 20 µM MK571 and incubated at 37 °C for 45 min. After incubation, the tubuloid epithelium was washed twice with PBS, dissociated using accutase + 10 µM Y-27632 (AbMole), washed, and resuspended in HBSS with 1% HEPES + 10 µM Y-27632 + DAPI and analyzed using a Fortessa™ flow cytometer (BD Biosciences). Median CDF fluorescence intensity (FI) was measured in DAPI-negative single cells using the [488]530_30 channel. % intracellular CDF was determined as (median FI/mean median FI in the minus MK571 control conditions)*100%.

Na^+ Reabsorption Experiments. iPSCod tubuloids were dissociated, grown to a confluent 2D monolayer in EM, and differentiated for 5 to 7 d as described above. Prior to the sodium uptake experiment, iPSCod tubuloids were preincubated for 30 min with either isotonic buffer (140 mM NaCl, 5 mM KCl, 1 mM $CaCl_2$, 1 mM $MgCl_2$, and 5 mM HEPES, with pH adjusted to 7.4 using Tris) or, to stimulate sodium uptake, hypotonic low-chloride buffer (70 mM Na^+ D-gluconate, 2.5 mM K^+ D-gluconate, 0.5 mM $CaCl_2$, 0.5 mM $MgCl_2$ and 2.5 mM HEPES, with pH set to 7.4 using Tris). The inhibitors (0.1 mM) hydrochlorothiazide, bumetanide, amiloride, and/or ouabain were included in the preincubation to inhibit the transporters/channels NCC, NKCC2, ENaC, and Na/K-ATPase, respectively. Ouabain was added to prevent basolateral removal of absorbed $^{22}Na^+$. Same buffers including the radioactive tracer $^{22}Na^+$ replaced the preincubation buffers and incubated for 30 min at 37 °C. The cells were washed three times in ice-cold isotonic or hypotonic buffer to remove any extracellular $^{22}Na^+$ and lysed using 0.05% SDS for 30 min at 37 °C. Intracellular $^{22}Na^+$ radioactivity was measured using a liquid scintillation counter (Hidex 300SL).

Statistics. Statistical analysis was performed using GraphPad Prism software. Unpaired *t* tests were used in all cases. ns = nonsignificant, $*P < 0.05$, $**P < 0.01$, $***P < 0.001$, $****P < 0.0001$.

Data, Materials, and Software Availability. All study data are included in the article and/or *SI Appendix*.

ACKNOWLEDGMENTS. F.A.Y.Y., C.M.E.A., C.P.C., R.M., M.B.R., and M.C.V. acknowledge the support of the partners of "Regenerative Medicine Crossing Borders" (RegMed XB), Powered by Health~Holland, Top Sector Life Sciences & Health and the Gravitation Program "Materials Driven Regeneration", funded by the Netherlands Organization for Scientific Research (024.003.013). J.J. is supported by the Netherlands Organisation for Scientific Research (NWO Veni grant no: 091 501 61 81 01 36) and the Dutch Kidney Foundation (grant no. 19OK005). We are grateful to H. Begthel (Hubrecht Institute, the Netherlands) for preparation of some of the immunohistochemistry samples.

Author affiliations: [a]Hubrecht Institute for Developmental Biology and Stem Cell Research - Royal Netherlands Academy of Arts and Sciences (KNAW) & University Medical Center Utrecht, 3584 CT and 3584 CX Utrecht, Netherlands; [b]Department of Nephrology and Hypertension, University Medical Center Utrecht, 3584 CX Utrecht, the Netherlands; [c]Department of Pathology, Radboud Institute for Molecular Life Sciences, Radboud University Medical Center, GA 6525 Nijmegen, The Netherlands; [d]Department of Pediatric Nephrology, Radboud Institute for Molecular Life Sciences, Radboud University Medical Center, Amalia Children's Hospital, GA 6525 Nijmegen, The Netherlands; [e]Institute of Experimental Medicine and Systems Biology, Rheinisch-Westfälische Technische Hogeschool (RWTH) Aachen University, 52074 Aachen, Germany; [f]Department of Physiology, Radboud Institute for Molecular Life Sciences, Radboud University Medical Center, GA 6525 Nijmegen, The Netherlands; and [g]Division of Pharmacology, Utrecht Institute for Pharmaceutical Sciences, Utrecht University, CG 3584 Utrecht, The Netherlands

Author contributions: F.A.Y.Y., J.J., C.M.E.A., E.D., C.P.C., R.M., J.G.H., B.S., M.B.R., M.C.V., and H.C. designed research; F.A.Y.Y., J.J., C.M.E.A., E.D., and C.P.C. performed research; F.A.Y.Y., J.J., C.M.E.A., E.D., C.P.C., R.M., J.G.H., B.S., M.B.R., M.C.V., and H.C. analyzed data; and F.A.Y.Y., J.J., C.M.E.A., E.D., C.P.C., R.M., J.G.H., B.S., M.B.R., M.C.V., and H.C. wrote the paper.

Reviewers: S.V., Kvantum Institute, Faculty of Biochemistry and Molecular Medicine, University of Oulu; and J.M.W., Cincinnati Children's Hospital Medical Center.

Competing interest statement: H.C. is head of Pharma Research and Early Development of Roche in Basel, Switzerland since March 2022. H.C. is inventor on several patents related to organoid technology; please see the full disclosure at https://www.uu.nl/staff/JCClevers/.

1. M. Takasato *et al.*, Kidney organoids from human iPS cells contain multiple lineages and model human nephrogenesis. *Nature* **526**, 564–568 (2015).
2. A. Taguchi, R. Nishinakamura, Higher-order kidney organogenesis from pluripotent stem cells. *Cell Stem Cell* **21**, 730–746.e6 (2017).
3. R. Morizane *et al.*, Nephron organoids derived from human pluripotent stem cells model kidney development and injury. *Nat. Biotechnol.* **33**, 1193–1200 (2015).
4. F. Schutgens *et al.*, Tubuloids derived from human adult kidney and urine for personalized disease modeling. *Nat. Biotechnol.* **37**, 303–313 (2019).
5. F. A. Yousef Yengej, J. Jansen, M. B. Rookmaaker, M. C. Verhaar, H. Clevers, Kidney organoids and tubuloids. *Cells* **9**, 1–20 (2020).
6. H. Wu *et al.*, Comparative analysis and refinement of human PSC-derived kidney organoid differentiation with single-cell transcriptomics. *Cell Stem Cell* **23**, 869–881.e8 (2018).

7. A. N. Combes, L. Zappia, P. X. Er, A. Oshlack, M. H. Little, Single-cell analysis reveals congruence between kidney organoids and human fetal kidney. *Genome. Med.* **11**, 3 (2019).
8. S. M. Czerniecki *et al.*, High-throughput screening enhances kidney organoid differentiation from human pluripotent stem cells and enables automated multidimensional phenotyping. *Cell Stem Cell* **22**, 929–940.e4 (2018).
9. B. S. Freedman *et al.*, Modelling kidney disease with CRISPR-mutant kidney organoids derived from human pluripotent epiblast spheroids. *Nat. Commun.* **6**, 8715 (2015).
10. C. W. Van Den Berg, A. Koudijs, L. Ritsma, T. J. Rabelink, In vivo assessment of size-selective glomerular sieving in transplanted human induced pluripotent stem cell-derived kidney organoids. *J. Am. Soc. Nephrol.* **31**, 921–929 (2020).
11. S. Kuraoka *et al.*, PKD1-dependent renal cystogenesis in human induced pluripotent stem cell-derived ureteric bud/collecting duct organoids. *J. Am. Soc. Nephrol.* **31**, 2355–2371 (2020).
12. S. E. Howden *et al.*, Plasticity of distal nephron epithelia from human kidney organoids enables the induction of ureteric tip and stalk. *Cell Stem Cell* **28**, 671–684.e6 (2021).
13. T. Shimizu *et al.*, A novel ADPKD model using kidney organoids derived from disease-specific human iPSCs. *Biochem. Biophys. Res. Commun.* **529**, 1186–1194 (2020).
14. M. Dvela-Levitt *et al.*, Small molecule targets TMED9 and promotes lysosomal degradation to reverse proteinopathy. *Cell* **178**, 521–535.e23 (2019).
15. T. A. Forbes *et al.*, Patient-iPSC-derived kidney organoids show functional validation of a ciliopathic renal phenotype and reveal underlying pathogenetic mechanisms. *Am. J. Hum. Genet.* **102**, 816–831 (2018).
16. V. Monteil *et al.*, Inhibition of SARS-CoV-2 infections in engineered human tissues using clinical-grade soluble human ACE2. *Cell* **181**, 905–913.e7 (2020).
17. J. Jansen *et al.*, SARS-CoV-2 infects the human kidney and drives fibrosis in kidney organoids. *Cell Stem Cell* **29**, 217–231.e8 (2022).
18. J. Jansen *et al.*, Human pluripotent stem cell-derived kidney organoids for personalized congenital and idiopathic nephrotic syndrome modeling. *Development* **149**, dev200198 (2022).
19. J. M. Vanslambrouck *et al.*, A toolbox to characterize human induced pluripotent stem cell-derived kidney cell types and organoids. *J. Am. Soc. Nephrol.* **30**, 1811–1823 (2019).
20. A. Przepiorski *et al.*, A simple bioreactor-based method to generate kidney organoids from pluripotent stem cells. *Stem Cell Rep.* **11**, 470–484 (2018).
21. J. H. Low *et al.*, Generation of human PSC-derived kidney organoids with patterned nephron segments and a de novo vascular network. *Cell Stem Cell* **25**, 373–387.e9 (2019).
22. C. W. van den Berg *et al.*, Renal subcapsular transplantation of PSC-derived kidney organoids induces neo-vasculogenesis and significant glomerular and tubular maturation in vivo. *Stem Cell Rep.* **10**, 751–765 (2018).
23. T. Geuens *et al.*, Thiol-ene cross-linked alginate hydrogel encapsulation modulates the extracellular matrix of kidney organoids by reducing abnormal type 1a1 collagen deposition. *Biomaterials* **275**, 120976 (2021).
24. S. V. Kumar *et al.*, Kidney micro-organoids in suspension culture as a scalable source of human pluripotent stem cell-derived kidney cells. *Development* **146**, dev172361 (2019).
25. A. Subramanian *et al.*, Single cell census of human kidney organoids shows reproducibility and diminished off-target cells after transplantation. *Nat. Commun.* **10**, 5462 (2019).
26. B. D. Humphreys *et al.*, Intrinsic epithelial cells repair the kidney after injury. *Cell Stem Cell* **2**, 284–291 (2008).
27. F. Schutgens *et al.*, Troy/TNFRSF19 marks epithelial progenitor cells during mouse kidney development that continue to contribute to turnover in adult kidney. *Proc. Natl. Acad. Sci. U.S.A.* **114**, E11190–E11198 (2017).
28. C. Calandrini *et al.*, An organoid biobank for childhood kidney cancers that captures disease and tissue heterogeneity. *Nat. Commun.* **11**, 1310 (2020).
29. A. Jamalpoor *et al.*, Cysteamine–bicalutamide combination therapy corrects proximal tubule phenotype in cystinosis. *EMBO Mol. Med.* **13**, e13067 (2021).
30. T. Ichimura *et al.*, KIM-1/TIM-1 is a receptor for SARS-CoV-2 in lung and kidney. MedRxiv Preprint Server for Health Sciences (2020), https://doi.org/10.1101/2020.09.16.20190694. Last accessed January 2023.
31. C. Wiraja *et al.*, Nephrotoxicity assessment with human kidney tubuloids using spherical nucleic acid-based mRNA nanoflares. *Nano Lett.* **21**, 5850–5858 (2021).
32. Y. Xu *et al.*, Adult human kidney organoids originate from CD24(+) cells and represent an advanced model for adult polycystic kidney disease. *Nat. Genet.* **54**, 1690–1701 (2022).
33. L. Gijzen *et al.*, Culture and analysis of kidney tubuloids and perfused tubuloid cells-on-a-chip. *Nat. Protoc.* **16**, 2023–2050 (2021), 10.1038/s41596-020-00479-w.
34. F. Schutgens, M. Rookmaaker, M. Verhaar, A perspective on a urine-derived kidney tubuloid biobank from patients with hereditary tubulopathies. *Tissue Eng. Part C Methods* **27**, 177–182 (2021).
35. J. R. Spence *et al.*, Directed differentiation of human pluripotent stem cells into intestinal tissue in vitro. *Nature* **470**, 105–109 (2011).
36. M. A. Lancaster *et al.*, Impaired Wnt-β-catenin signaling disrupts adult renal homeostasis and leads to cystic kidney ciliopathy. *Nat. Med.* **15**, 1046–1054 (2009).
37. Y. Rinkevich *et al.*, In vivo clonal analysis reveals lineage-restricted progenitor characteristics in mammalian kidney development, maintenance, and regeneration. *Cell Rep.* **7**, 1270–1283 (2014).
38. H. D. Humes, D. A. Cieslinski, T. M. Coimbra, J. M. Messana, C. Galvao, Epidermal growth factor enhances renal tubule cell regeneration and repair and accelerates the recovery of renal function in postischemic acute renal failure. *J. Clin. Invest.* **84**, 1757–1761 (1989).
39. C. Pou Casellas *et al.*, Regulation of solute carriers oct2 and OAT1/3 in the kidney: A phylogenetic, ontogenetic, and cell dynamic perspective. *Physiol. Rev.* **102**, 993–1024 (2022).
40. M. H. Little, S. V. Kumar, T. Forbes, Recapitulating kidney development: Progress and challenges. *Semin. Cell Dev. Biol.* **91**, 153–168 (2019).
41. N. Barker *et al.*, Lgr5+ve stem/progenitor cells contribute to nephron formation during kidney development. *Cell Rep.* **2**, 540–552 (2012).
42. R. D. Toto, Conventional measurement of renal function utilizing serum creatine, creatine clearance, inulin and para-aminohippuric acid clearance. *Curr. Opin. Nephrol. Hypertens.* **4**, 505–509 (1995).
43. J. Jansen *et al.*, Bioengineered kidney tubules efficiently excrete uremic toxins. *Sci. Rep.* **6**, 26715 (2016).
44. M. J. Zamek-Gliszczynski *et al.*, Pharmacokinetics of 5 (and 6)-carboxy-2′,7′-dichlorofluorescein and its diacetate promoiety in the liver. *J. Pharmacol. Exp. Ther.* **304**, 801–809 (2003).
45. C. J. Z. Richardson *et al.*, Activation of the thiazide-sensitive Na+-Cl- cotransporter by the WNK-regulated kinases SPAK and OSR1. *J. Cell Sci.* **121**, 675–684 (2008).
46. A. Taruno, N. Niisato, Y. Marunaka, Hypotonicity stimulates renal epithelial sodium transport by activating JNK via receptor tyrosine kinases. *Am. J. Physiol. Ren. Physiol.* **293**, F128–F138 (2007).
47. A. Hannemann, P. W. Flatman, Phosphorylation and transport in the Na-K-2Cl cotransporters, NKCC1 and NKCC2A, compared in HEK-293 cells. *PLoS One* **6**, e17992 (2011).
48. K. Uchimura, H. Wu, Y. Yoshimura, B. D. Humphreys, Human pluripotent stem cell-derived kidney organoids with improved collecting duct maturation and injury modeling. *Cell Rep.* **33**, 108514 (2020).
49. Z. Zeng *et al.*, Generation of patterned kidney organoids that recapitulate the adult kidney collecting duct system from expandable ureteric bud progenitors. *Nat. Commun.* **12**, 3641 (2021).
50. Y. Yoshimura *et al.*, Manipulation of nephron-patterning signals enables selective induction of podocytes from human pluripotent stem cells. *J. Am. Soc. Nephrol.* **30**, 304–321 (2019).
51. M. Shi *et al.*, Human ureteric bud organoids recapitulate branching morphogenesis and differentiate into functional collecting duct cell types. *Nat. Biotechnol.*, 10.1038/s41587-022-01429-5 (2022).
52. J. Y. C. Soo, J. Jansen, R. Masereeuw, M. H. Little, Advances in predictive in vitro models of drug-induced nephrotoxicity. *Nat. Rev. Nephrol.* **14**, 378–393 (2018).
53. B. S. Freedman, Physiology assays in human kidney organoids. *Am. J. Physiol. Renal Physiol.* **322**, F625–F638 (2022).
54. N. Montalbetti *et al.*, Functional characterization of ion channels expressed in kidney organoids derived from human induced pluripotent stem cells. *Am. J. Physiol. Renal Physiol.* **323**, F479–F491 (2022), 10.1152/ajprenal.00365.2021.
55. N. V. Kaverina *et al.*, Dual lineage tracing shows that glomerular parietal epithelial cells can transdifferentiate toward the adult podocyte fate. *Kidney Int.* **96**, 597–611 (2019).
56. S. J. Shankland, B. S. Freedman, J. W. Pippin, Can podocytes be regenerated in adults? *Curr. Opin. Nephrol. Hypertens.* **26**, 154–164 (2017).
57. L. J. Hale *et al.*, 3D organoid-derived human glomeruli for personalised podocyte disease modelling and drug screening. *Nat. Commun.* **9**, 5167 (2018).
58. R. Morizane, J. V. Bonventre, Generation of nephron progenitor cells and kidney organoids from human pluripotent stem cells. *Nat. Protoc.* **12**, 195–207 (2017).
59. Y. Xia *et al.*, The generation of kidney organoids by differentiation of human pluripotent cells to ureteric bud progenitor-like cells. *Nat. Protoc.* **9**, 2693–2704 (2014).
60. M. K. Vormann *et al.*, Modelling and prevention of acute kidney injury through ischemia and reperfusion in a combined human renal proximal tubule/blood vessel-on-a-chip. *Kidney360* **3**, 217–231 (2022).
61. V. V. T. Nguyen *et al.*, A human kidney and liver organoid-based multi-organ-on-a-chip model to study the therapeutic effects and biodistribution of mesenchymal stromal cell-derived extracellular vesicles. *J. Extracell. Vesicles* **11**, e12280 (2022).
62. P. A. Ortiz, cAMP increases surface expression of NKCC2 in rat thick ascending limbs: Role of VAMP. *Am. J. Physiol. Ren. Physiol.* **290**, F608–F616 (2006).
63. M. Huch *et al.*, Long-term culture of genome-stable bipotent stem cells from adult human liver. *Cell* **160**, 299–312 (2015).
64. H. Hu *et al.*, Long-term expansion of functional mouse and human hepatocytes as 3D organoids. *Cell* **175**, 1591–1606.e19 (2018).